Assessing the Influence of Large-Scale Environmental Conditions on the Rainfall Structure of Atlantic Tropical Cyclones: An Observational Study

DASOL KIM,[a] CHANG-HOI HO,[a] HIROYUKI MURAKAMI,[b] AND DOO-SUN R. PARK[c]

[a] *School of Earth and Environmental Sciences, Seoul National University, Seoul, South Korea*
[b] *NOAA/Geophysical Fluid Dynamics Laboratory, Princeton, New Jersey*
[c] *Department of Earth Science Education, Kyungpook National University, Daegu, South Korea*

(Manuscript received 20 May 2020, in final form 30 November 2020)

ABSTRACT: Understanding the mechanisms related to the variations in the rainfall structure of tropical cyclones (TCs) is crucial in improving forecasting systems of TC rainfall and its impact. Using satellite precipitation and reanalysis data, we examined the influence of along-track large-scale environmental conditions on inner-core rainfall strength (RS) and total rainfall area (RA) for Atlantic TCs during the TC season (July–November) from 1998 to 2019. Factor analysis revealed three major factors associated with variations in RS and RA: large-scale low and high pressure systems [factor 1 (F1)]; environmental flows, sea surface temperature, and humidity [factor 2 (F2)]; and maximum wind speed of TCs [factor 3 (F3)]. Results from our study indicate that RS increases with an increase in the inherent primary circulation of TCs (i.e., F3) but is less affected by large-scale environmental conditions (i.e., F1 and F2), whereas RA is primarily influenced by large-scale low and high pressure systems (i.e., F1) over the entire North Atlantic and partially influenced by environmental flows, sea surface temperature, humidity, and maximum wind speed (i.e., F2 and F3). A multivariable regression model based on the three factors accounted for the variations of RS and RA across the entire basin. In addition, regional distributions of mean RS and RA from the model significantly resembled those from observations. Therefore, our study suggests that large-scale environmental conditions over the North Atlantic Ocean are important predictors for TC rainfall forecasts, particularly with regard to RA.

KEYWORDS: Atmosphere; Atlantic Ocean; Rainfall; Tropical cyclones; Satellite observations

1. Introduction

Atlantic Ocean tropical cyclones (TCs), with their strong winds and heavy rainfall, represent severe meteorological disasters that threaten the United States of America (Rappaport 2000, 2014; Pielke et al. 2003; Czajkowski et al. 2011, 2017). Flooding caused by rainfall due to TCs is the most frequent among TC hazards (Rappaport 2000, 2014). Moreover, approximately 90% of deaths caused by TCs are due to drowning from storm surges, freshwater floods, and marine incidents (49%, 27%, and 12%, respectively; Rappaport 2014), which highlights the danger of water-related disasters caused by TCs. According to Czajkowski et al. (2011), a 1-in. (2.54 cm) increase in TC rainfall and a 1-kt (0.51 m s^{-1}) increase in TC wind resulted in an increase of total fatalities by 28% and 4%, respectively. Globally, other countries are also at risk of the dangers associated with TC rainfall (Park et al. 2015; Bakkensen et al. 2018). To prevent catastrophes by TCs, deep understanding and accurate prediction of TC rainfall is required.

Fundamentally, TC rainfall is the product of secondary circulation (i.e., radial and vertical motion), which is induced by primary circulation (i.e., horizontal and cyclonic motion) and friction in the boundary layer (Smith et al. 2009; Smith and Montgomery 2010; Montgomery and Smith 2017). Thus, TC rainfall generally increases with an increase in TC intensity (Rodgers et al. 1994; Lonfat et al. 2004; Jiang et al. 2008a; Lin et al. 2015; Rios Gaona et al. 2018). On the other hand, TC rainfall can also be affected by the surrounding environmental conditions. For example, TC rainfall can increase as sea surface temperature (SST) and humidity increase, as both are major sources of TC rainfall (Jiang et al. 2008b; Hill and Lackmann 2009; Matyas 2010; Lin et al. 2015). Moreover, environmental flows including steering flow and vertical wind shear are major causes of the asymmetry of TC rainfall (Frank and Ritchie 1999, 2001; Corbosiero and Molinari 2002, 2003; Chen et al. 2006). Kim et al. (2018) also suggested that environmental flows can play an important role in the changes in rainfall area of TCs, as rainfall areas expand with increasing asymmetry. Large-scale upper-level troughs are closely related to TC rainfall (Kim et al. 2006, 2019) as well as TC intensification (Molinari and Vollaro 1989; DeMaria et al. 1993; Hanley et al. 2001; Ritchie and Elsberry 2003) by providing angular momentum and upper-level divergence, which enhance cyclonic circulation and convection in TCs. In addition, topography can significantly affect both TC rainfall rate and structure during landfall periods by changing the friction and moisture of the surface and inducing forced ascents (Chen and Yau 2003; Park and Lee 2007; Kimball 2008; Xu et al. 2014).

Although many studies have suggested various mechanisms related to the variations in TC rainfall, relatively few studies have investigated the influence of environmental conditions on

Supplemental information related to this paper is available at the Journals Online website: https://doi.org/10.1175/JCLI-D-20-0376.s1.

Corresponding author: Chang-Hoi Ho, hoch@cpl.snu.ac.kr

DOI: 10.1175/JCLI-D-20-0376.1

TC rainfall based on large samples from observation (Jiang et al. 2008b; Konrad and Perry 2010; Matyas 2010, 2013, 2014; Lin et al. 2015; Kim et al. 2018; Zhou and Matyas 2018; Zhou et al. 2018). For example, Jiang et al. (2008b) reported that environmental moisture parameters such as total precipitable water, horizontal moisture convergence, and ocean surface moisture flux account for 26%–35% of the variability in volumetric rain (total volume of rainfall within a 5° radius from TC center) of Atlantic landfalling TCs from 1998 to 2006. According to Lin et al. (2015), both the maximum rainfall rates and radii of global TCs during 1998–2008 increased by 2.5 mm h^{-1} and 100 km, respectively, as the relative SST (anomalous SST relative to the tropical mean SST) increased by 3°C. Moreover, Kim et al. (2018) showed that the rainfall area of TCs over subtropical oceans increased by approximately 10^5 km^2 as the TC moving speed and vertical wind shear increased by 3 and 8 m s^{-1}, respectively, based on satellite observed precipitation data over 17 years.

In addition, TC rainfall can be affected by combined effects of multiple environmental conditions. Several studies examined the relationship between TC rainfall and multiple environmental conditions to find out which conditions had the greatest influence on TC rainfall (Konrad and Perry 2010; Matyas 2010, 2013, 2014; Zhou and Matyas 2018; Zhou et al. 2018). A number of works by Matyas have highlighted vertical wind shear and moisture among environmental conditions that determine extent of rain field during TC landfall in United States (Matyas 2010, 2013, 2014). Moreover, Zhou et al. (2018) suggested that the total precipitable water and upper-tropospheric divergence are the strongest predictors of rain field size for TCs landfalling over the eastern United States using statistical models. Previous research, however, focused on landfall TCs and did not cover TCs of the entire North Atlantic and recent period. In addition, environmental conditions that affect TC rainfall may not be independent of each other, but the relationship between environmental conditions has not been discussed in detail.

In this study, we examine the rainfall structure of TCs over the North Atlantic in terms of inner-core rainfall strength (RS) and total rainfall area (RA) using satellite precipitation data for the TC seasons (from July through November) from 1998 to 2019. Near the TC center, narrow but strong precipitation occurs in the eyewall clouds, whereas precipitation in the outer regions is relatively weak but appears over wide areas of spiral rainbands and anvil clouds (Houze 2010). The rainfall in the inner core accounts for 20%–35% of the total rainfall in a TC (Cerveny and Newman 2000). Therefore, the rainfall intensity and area have been widely used as indicators representing the rainfall structure of TCs (Jiang et al. 2008a; Matyas 2010, 2013, 2014; Lin et al. 2015; Rios Gaona et al. 2018; Zhou and Matyas 2018; Zhou et al. 2018). To identify independent and major factors affecting TC rainfall, multiple dynamic and thermodynamic environmental conditions surrounding TCs were classified into independent factors using factor analysis. Furthermore, a multivariable regression model based on the major factors found was used to quantify the relative contribution of each factor to the total variation in TC rainfall structure.

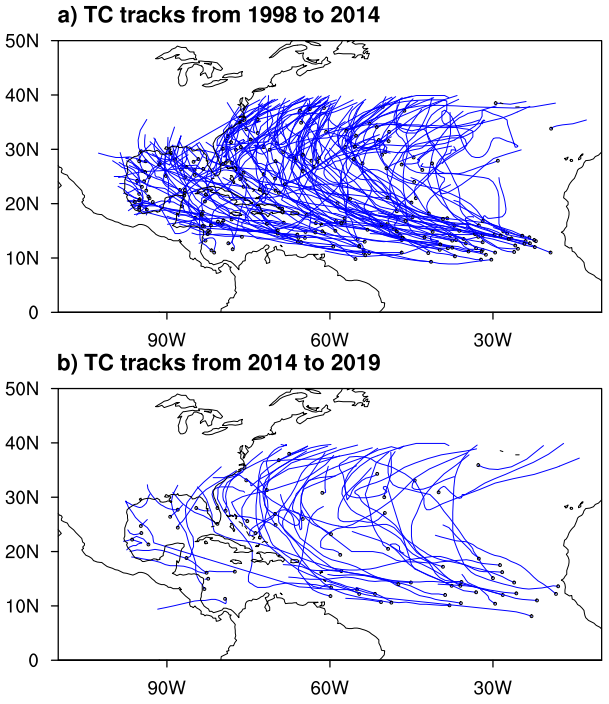

FIG. 1. Distribution of TC tracks from July to November over (a) 1998–2014 and (b) 2014–19.

Section 2 describes the data and methods used in this study, and statistical results related to the rainfall structure of Atlantic TCs are presented in section 3. In section 4, we explore the major factors associated with changes in rainfall structure of TCs, whereas in section 5 the influence of these factors on TC rainfall is investigated. In section 6 we discuss and summarize the findings of our study.

2. Data and methods

Best-track data, providing center locations, maximum wind speed V_{max}, and grade of TCs in 6-h intervals were obtained from the Hurricane Database (HURDAT) of the International Best Track Archive for Climate Stewardship (IBTrACS v03r09; Knapp et al. 2010). Tropical depressions and extratropical cyclones were excluded from the analysis based on the TC classification (grade) in the best-track data. The rainfall structure of a TC was analyzed using precipitation data from the Tropical Rainfall Measuring Mission (TRMM) 3B42 (Huffman et al. 2007) and Global Precipitation Measurement (GPM) IMERG V06 (Integrated Multi-Satellite Retrievals for GPM, version 06; Huffman et al. 2019). The TRMM covers the North Atlantic up to 50°N with spatial and temporal resolutions of 0.25° and 3 h, respectively. The IMERG covers the North Atlantic up to 60°N with spatial and temporal resolutions of 0.1° and 30 min, respectively. Since the two precipitation datasets are provided in different periods, TRMM and IMERG data were used for the analysis periods from July to November over 1998–2014 and 2014–19, respectively. Figure 1 presents the distribution of TC tracks for the two periods analyzed in this study.

Using the TRMM and IMERG data, we calculated RS and RA representing the intensity and spatial scale of TC rainfall, respectively. RS was defined as the mean rainfall rate within a 200-km radius from the TC center. TC rainfall peaks within a 100-km radius and decreases rapidly to 200 km (Jiang et al. 2008a; Lin et al. 2015; Rios Gaona et al. 2018). We tested RS using different radius criteria from 100 to 200 km, and the overall result was not significantly different, except that the smaller the radius criterion was, the larger the RS was (see Table S1 in the online supplemental material). RA was defined as the total area of all rain cells related to the TC. A rain cell, a continuum of grid boxes with a precipitation rate exceeding 0.5 mm h^{-1}, was regarded to be associated with the TC if the minimum distance between the cell and the TC center was less than 500 km (Kim et al. 2018, 2019). In the calculations of RS and RA, both land and ocean grid cells were used without distinction, and original TRMM and IMERG data were used without interpolation. Both RS and RA were sampled every 6 h at the given locations of the TC centers, and the number of samples from TRMM and IMERG was 4407 and 1457, respectively.

Large-scale environmental conditions surrounding TCs were examined using the daily Optimum Interpolation SST, version 2 (OISSTv2; Reynolds et al. 2002) and reanalysis data from the European Centre for Medium-Range Weather Forecasts (ECMWF), specifically ERA5 (Hersbach et al. 2020). OISSTv2 and ERA5 reanalysis data have a horizontal resolution of 0.25° and are available from 1981 and 1979 to the present, respectively. The environmental conditions investigated in this study included SST, relative humidity at 600 hPa (RH600), relative vorticity at 850 hPa (RV850), divergence at 850 and 200 hPa (DV850 and DV200, respectively), vertical wind shear between 850 and 200 hPa (VWS), and steering flow (STF; i.e., pressure-weighted mean winds from 900 to 100 hPa). The selection of these dynamic and thermodynamic environmental conditions was based on previous studies (Hanley et al. 2001; Matyas 2010, 2013, 2014; Lin et al. 2015; Kim et al. 2018; Zhou et al. 2018). To obtain large-scale environmental conditions surrounding TCs, 3-day low-pass filtering was applied to the original large-scale variables (Fu et al. 2012; Peng et al. 2012). Then, the filtered large-scale variables were averaged within a 1000-km radius from the TC center. The overall results were not very sensitive to the period of the low-pass filter and radius criteria used (Figs. S1 and S2 in the online supplemental material). In addition to large-scale environmental conditions, TC rainfall structure is also closely related to the inherent circulation of the TC. Thus, the relationship between TC rainfall and V_{max}, representing the strength of the primary circulation, was also examined.

As TCs are affected by multiple environmental conditions that may not be independent of one other, a factor analysis (Woods and Edwards 2008) was applied to large-scale environmental conditions and V_{max} to identify independent and major factors affecting TC rainfall. Factor analysis is a statistical method analogous to principal component analysis and is used to find latent variables, or factors, that explain the common variance within a set of variables. The eigenvalue of each factor is the sum of the squared factor loadings, which are the correlation coefficients between the factor and the analyzed variables. If a factor has a large eigenvalue, the factor accounts for a large portion of common variance in the variables. As the factors are found in the order of their eigenvalues and set to be orthogonal to each other, they are independent of one other. Factors with an eigenvalue greater than 1 were interpreted using the Kaiser criterion and analyzed variables were normalized, as the units of the variables differed from one another.

3. Statistics of rainfall structure of Atlantic tropical cyclones

First, we investigated the basic properties of TC rainfall, including the mean precipitation rate and distribution relative to the TC center (Figs. 2a,b). Rainfall fields of each sample were rotated so that the direction of TC motion was oriented toward the top of the figure. Our results indicate that rainfall rate was maximized in the inner-core region (within 200 km from the center; dashed circle in Figs. 2a and 2b) and decreased outwards from the TC center. The maximum rainfall rate was 5.01 and 6.71 mm h^{-1} for the TRMM and IMERG, respectively, and appeared in the front-right quadrant of the TC center, which is consistent with results from other studies (Lonfat et al. 2004; Jiang et al. 2008a; Villarini et al. 2014; Rios Gaona et al. 2018). The radius of maximum rainfall was 62.1 and 59.8 km for the TRMM and IMERG, respectively. The occurrence frequencies of RS and RA generally followed lognormal distributions (Figs. 2c–f). Notably, the wind radii of TCs also show a lognormal distribution according to Chavas and Emanuel (2010). For the TRMM, the mean values of RS and RA were 2.88 mm h^{-1} and 3.66 × 10^5 km^2, respectively. For the IMERG, the mean values of RS and RA were 3.46 mm h^{-1} and 2.94 × 10^5 km^2, respectively. The RA calculated in this study is similar to those in Lin et al. (2015) and Kim et al. (2018), but larger than those in Matyas (2014) and Zhou et al. (2018), which used higher rainfall criterion (2.5 mm h^{-1}) to obtain RA. The mean values of RA for the TRMM and IMERG correspond to the area of a circles with radii of 341 and 306 km, respectively. These are larger than typical size parameters of TC winds, which are approximately 200, 240, and 274 km for radii of 17, 15, and 12 m s^{-1} wind speed, respectively (Liu and Chan 2002; Kimball and Mulekar 2004; Chan and Chan 2015; Chavas et al. 2016).

Figure 3 represents the spatial distributions of mean RS and RA values over the North Atlantic. Notably, RS and RA varied substantially within the basin. For example, high RS values appeared over the Gulf of Mexico, the Caribbean Sea, and east of the West Indies (15°–25°N, 55°–90°W) (Figs. 2a,b). In addition, RA values were highest over the tropics west of 60°W and midlatitudes near 60°W (Figs. 2c,d). Notably, the spatial pattern of RA over the eastern United States in this study is similar to that in Zhou et al. (2018), except for the magnitudes. For the TRMM, the mean RS and RA in each grid box varied from 0.89 to 4.81 mm h^{-1} and from 1.23 × 10^5 to 6.91 × 10^5 km^2, respectively. For the IMERG, the mean RS and RA in each grid box varied from 0.77 to 8.20 mm h^{-1} and from 1.20 × 10^5 to 7.23 × 10^5 km^2, respectively. Although both RS and RA showed large

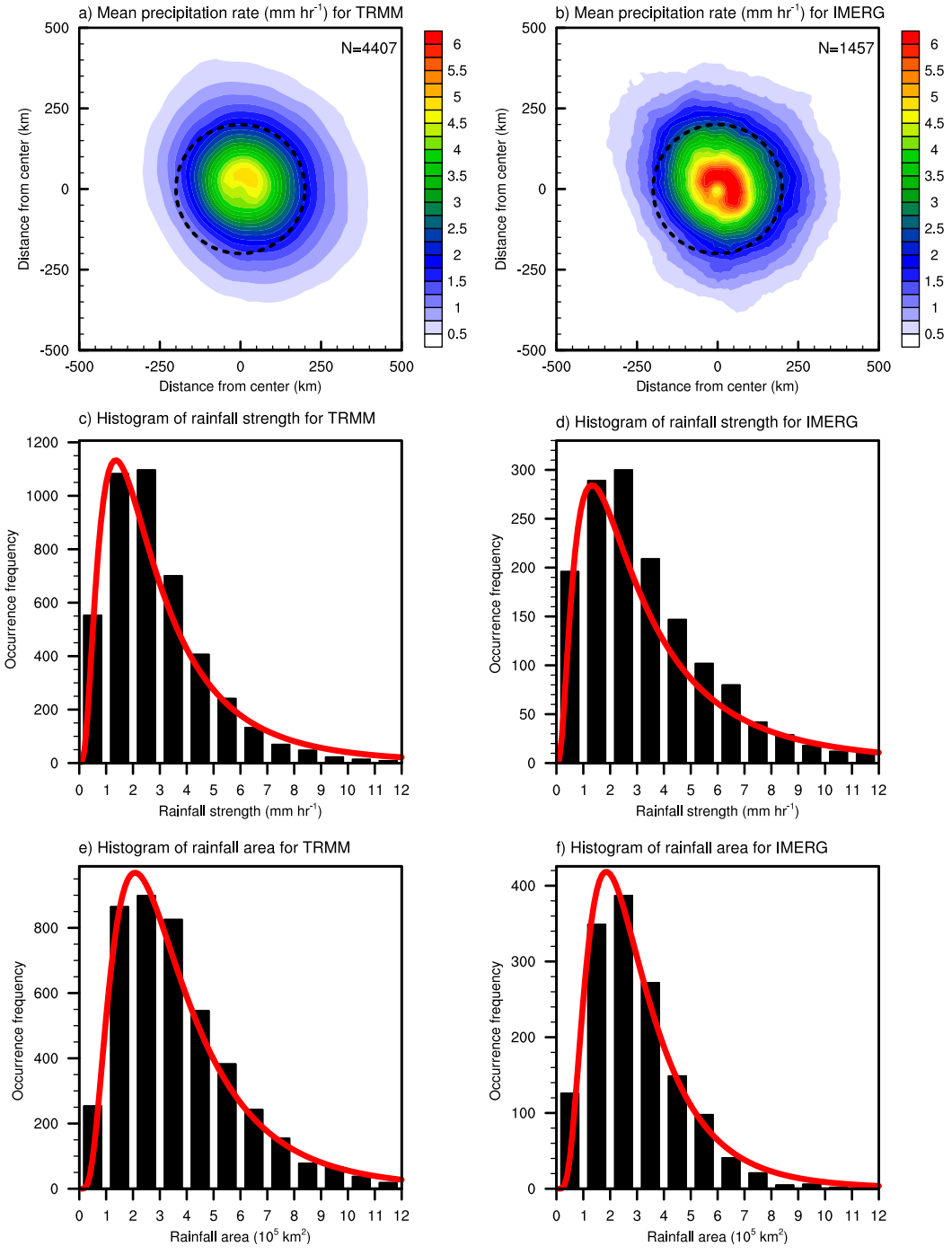

FIG. 2. (a),(b) Mean tropical cyclone (TC) rainfall distribution, and histograms of (c),(d) rainfall strength and (e),(f) rainfall area obtained from the (left) TRMM and (right) IMERG. The black dashed circle in (a) and (b) represents the inner-core region of a TC, and red curves in (c)–(f) indicate lognormal fits of RS or RA.

variability in space, the one-to-one relationship between them was very weak (correlation coefficient $r = 0.09$), indicating that they may be controlled by different factors. It is notable that the relationship between intensity and spatial scale of TC wind (e.g., V_{max} and radius of 17 m s^{-1}) is also weak (Merrill 1984; Weatherford and Gray 1988; Chavas and Emanuel 2010; Chavas et al. 2015, 2016).

We compared the results from the TRMM and IMERG for 2014, where the periods of the two datasets overlap (Table 1). The mean RS of TRMM was 26.8% smaller than that of IMERG. The

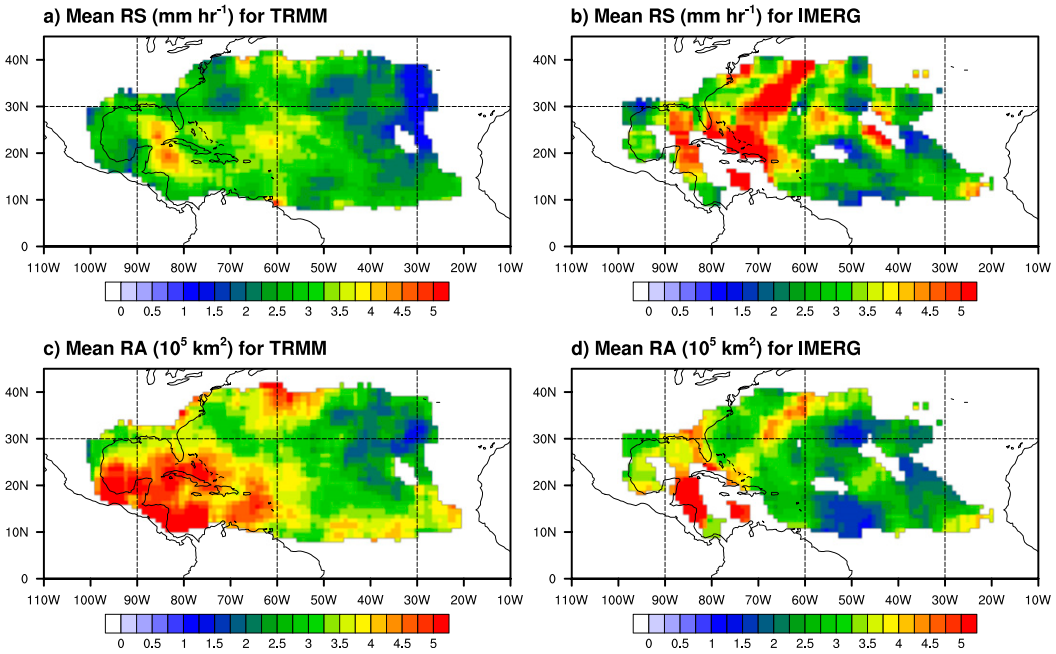

FIG. 3. Distribution of (a),(b) rainfall strength (RS) and (c),(d) rainfall area (RA) for (left) TRMM and (right) IMERG averaged in 5° square window according to the samples' TC center locations. Only grid points with a sample number of larger than 10 are shown.

correlation coefficient for RS between TRMM and IMERG was 0.61. On the other hand, the difference in RA between TRMM and IMERG was only 12.1%, and their correlation coefficient was 0.81. Therefore, the difference between TRMM and IMERG appeared to be more pronounced with stronger precipitation in the inner core, which may be attributed to the difference in resolution of the two datasets (Rios Gaona et al. 2018). On the other hand, the results of the IMERG may be biased by specific samples due to the short analysis period of the IMERG. For example, RS of the IMERG showed subsequently high values over the northeastern region from the Bahamas, which is associated with strong TCs (above category 1) passing through that region more frequently (Fig. S3 in the online supplemental material). Despite the difference between the two datasets, the overall characteristics of TC rainfall were similar, which will be discussed in detail below.

4. Major factors affecting tropical cyclone rainfall

To examine the variations in RS and RA according to large-scale environmental conditions, the one-to-one relationships between TC rainfall structure variables (i.e., RS and RA) and each environmental condition were investigated (Fig. 4), together with the relationship between TC rainfall structure and V_{max}, for comparative purposes. Notably, the results of TRMM and IMERG are consistent despite the different resolutions and analysis periods. RS showed the highest correlation coefficient r with V_{max} (r = 0.57 for TRMM and 0.56 for IMERG, respectively). The relationship between RS and the large-scale environmental variables, except for VWS, was statistically significant at the 95% confidence level (r ranging from −0.16 to 0.31 for TRMM and from −0.23 to 0.27 for IMERG, respectively) but much weaker than that between RS and V_{max}. Contrary to RS, RA was strongly correlated to large-scale environmental conditions including RH600, RV850, DV850, and DV200 (r ranging from −0.57 to 0.68 for TRMM and from −0.50 to 0.62 for IMERG, respectively) and showed a weaker relationship with V_{max} (r = 0.17 for TRMM and 0.20 for IMERG, respectively; significant at the 95% confidence level). These results indicate that RS is largely dependent on V_{max}, whereas RA is more dependent on large-scale environmental conditions.

TABLE 1. Statistics of rainfall strength and rainfall area obtained from the TRMM and IMERG for 2014.

	RS	RA
Mean of TRMM	3.31 mm h^{-1}	3.36 mm h^{-1}
Mean of IMERG	4.53×10^5 km^2	3.00×10^5 km^2
Ratio of mean (TRMM/IMERG; %)	73.2	112.1
Correlation between TRMM and IMERG	0.61	0.81

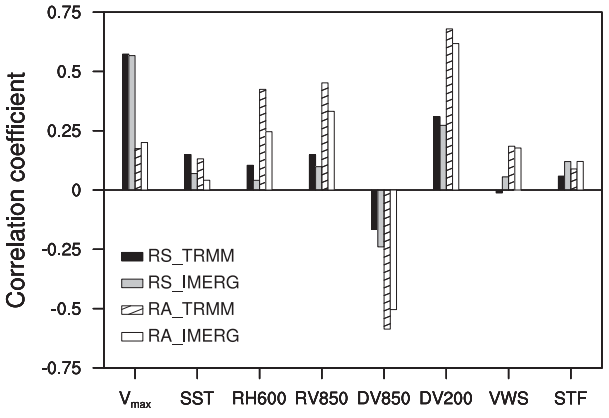

FIG. 4. Correlation coefficients between TC rainfall structure and the seven environmental variables plus V_{max}. The black bars and striped bars indicate the results of rainfall strength and rainfall area, respectively, obtained from the TRMM. The gray bars and white bars indicate the results of rainfall strength and rainfall area, respectively, obtained from the IMERG.

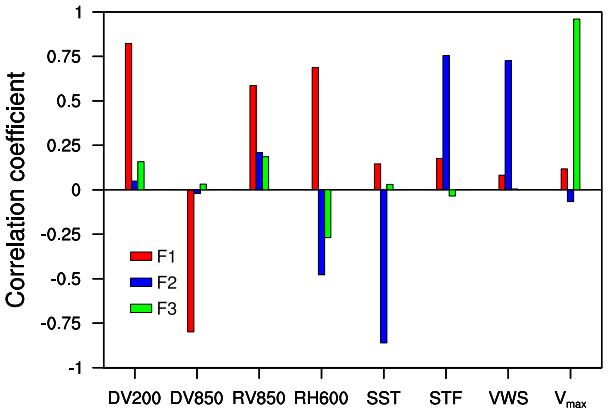

FIG. 5. Correlation coefficients between three significant factors (F1, F2, and F3, represented by red, blue, and green bars, respectively) and the seven environmental variables plus V_{max}.

The close relationship between rainfall rate in the inner core of TCs and V_{max} is consistent with that reported in previous studies (Rodgers et al. 1994; Lonfat et al. 2004; Jiang et al. 2008a; Lin et al. 2015; Rios Gaona et al. 2018). According to Jiang et al. (2008a), the rainfall rate within a 200-km radius from the TC center is strongly correlated with V_{max} (r = 0.39–0.68), but the relationship rapidly weakens with an increase in radius. As shown in section 3, the relationship between RS and RA is very weak, indicating that RA is closely related to rainfall structure in the outer regions of TCs. This is confirmed by RA relating more closely to environmental conditions than V_{max}. The RA increased with an increase in RH600 (i.e., positive relationship) because of an increase in moisture availability. Large-scale angular momentum (i.e., RV850; positive relationship) and low-level convergence and upper-level divergence (i.e., DV850 and DV200; negative and positive relationship, respectively) have been reported to increase the vertical circulation and intensity of TCs (Molinari and Vollaro 1989; DeMaria et al. 1993; Hanley et al. 2001; Ritchie and Elsberry 2003). Several studies showed the intensification of TC rainfall with an increase in SST (Scoccimarro et al. 2014; Villarini et al. 2014; Lin et al. 2015). Our results suggest that SST can increase both RS and RA; however, the contribution of SST to changes in RS and RA was much smaller than that of V_{max} and other environmental conditions (Fig. 4).

TABLE 2. Eigenvalue and explained variance matrix for the seven environmental conditions and V_{max}. The eigenvalue is the total sum of squared factor loadings representing the correlation coefficients between each factor and the analyzed variables. Explained variance is the ratio of each eigenvalue to the total eigenvalue. According to the Kaiser criterion, meaningful factors have an eigenvalue of greater than 1.

Factor	Eigenvalue	Explained variance (%)
F1	2.27	28.4
F2	2.08	26.0
F3	1.03	12.9
F4	0.76	9.5
F5	0.73	9.1
F6	0.49	6.2
F7	0.34	4.2
F8	0.30	3.7

To identify independent factors associated with variations in RS and RA, factor analysis was applied to all seven environmental variables (SST, RH600, RV850, DV850, DV200, VWS, and STF) as well as V_{max}. The analysis showed that three significant factors with eigenvalues greater than one accounted for 67.3% of the total variability of all eight analyzed variables (Table 2). The first two factors related to variations of large-scale environmental conditions, with factor 1 (F1) showing significant relationships with RV850, RH600, DV850, and DV200 (red bars in Fig. 5, with r ranging from −0.80 to 0.82), and factor 2 (F2) associated with variations of SST, RH600, VWS, and STF (blue bars in Fig. 5, with r ranging from −0.86 to 0.76). These results indicate that TCs are influenced by multiple and simultaneously varying environmental conditions. Last, factor 3 (F3) showed a significant relationship with only V_{max} (green bars in Fig. 5). Because the correlation coefficient between F3 and V_{max} was 0.96, F3 can be regarded as V_{max}.

To understand the meaning of each factor, variations of the analyzed variables closely related to each factor were examined. Figure 6 represents variations of RV850, RH600, DV850, and DV200 according to F1. When F1 was high (i.e., F1 greater than the mean value plus one standard deviation), anomalous large-scale cyclonic circulations in the lower troposphere appeared over the Caribbean Sea (Fig. 6a). Along with an increase in cyclonic circulation, relative humidity, convergence in the lower troposphere, and divergence in the upper troposphere also significantly increased over the Caribbean Sea

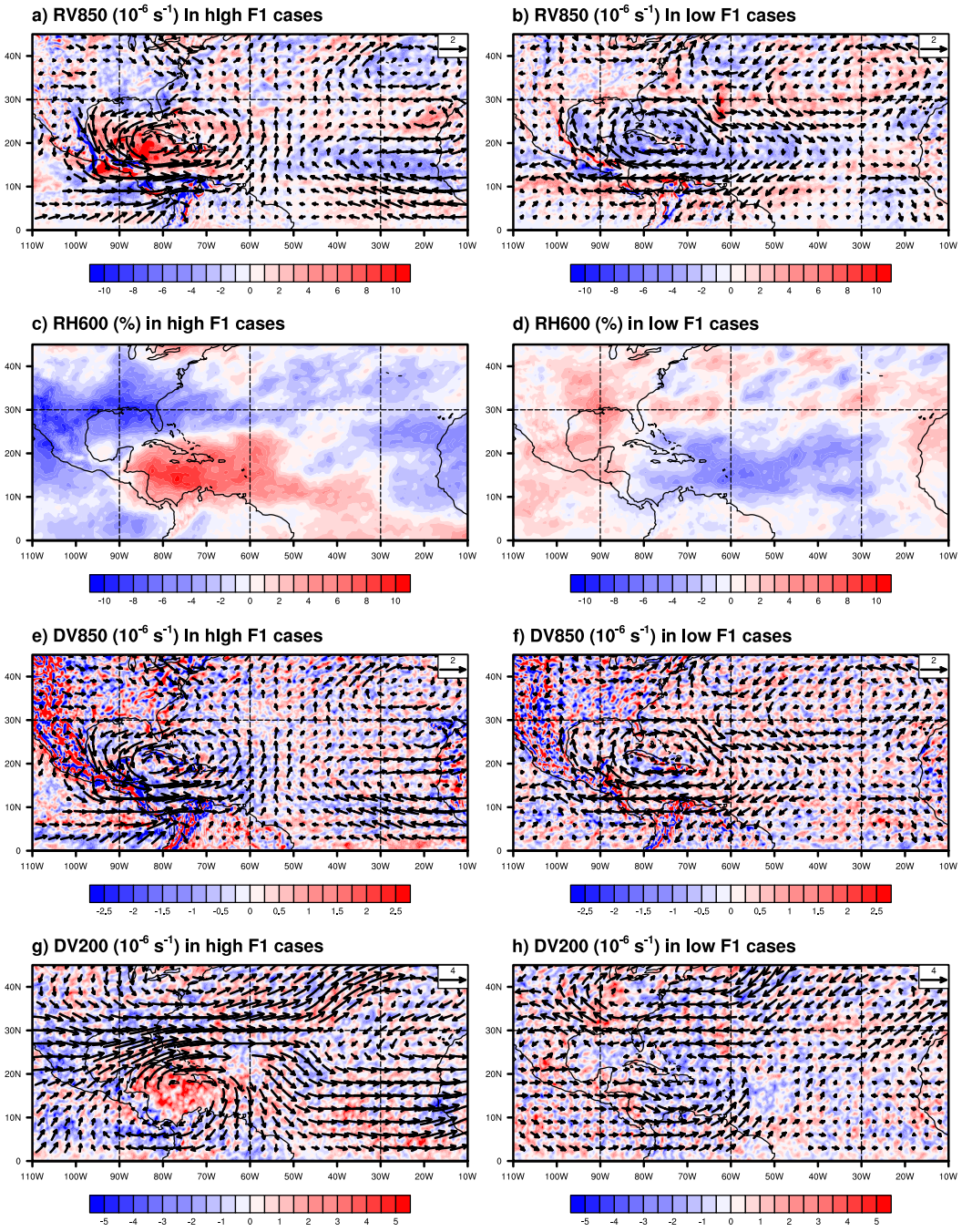

FIG. 6. Climatological anomaly composites of (a),(b) RV850 (shading), (c),(d) RH600, (e),(f) DV850 (shading), and (g),(h) DV200 (shading) for the (left) high-F1 and (right) low-F1 cases. Arrows represent wind vectors at 850- or 200-hPa levels, as labeled. High-F1 cases are defined as F1 greater than the mean value plus 1 standard deviation of F1. Low-F1 cases are defined as F1 less than the mean value minus 1 standard deviation of F1. Only differences that are significant at the 95% confidence level by Student's *t* test are presented.

and central part of North Atlantic (Figs. 6c,e,g). When F1 is low, the opposite pattern appeared (right column in Fig. 6). Therefore, variations of F1 represent changes in large-scale low and high pressure systems. Similarly, SST, RH600, VWS, and STF varied significantly according to F2 (Fig. 7). When F2 was high (i.e., F2 greater than the mean value plus 1 standard deviation), SST and RH600 decreased significantly above 20°N (Figs. 7a,c), whereas westerly VWS and STF increased (Figs. 7e,g), and the opposite was true when F2 was low (i.e., F2 less than the

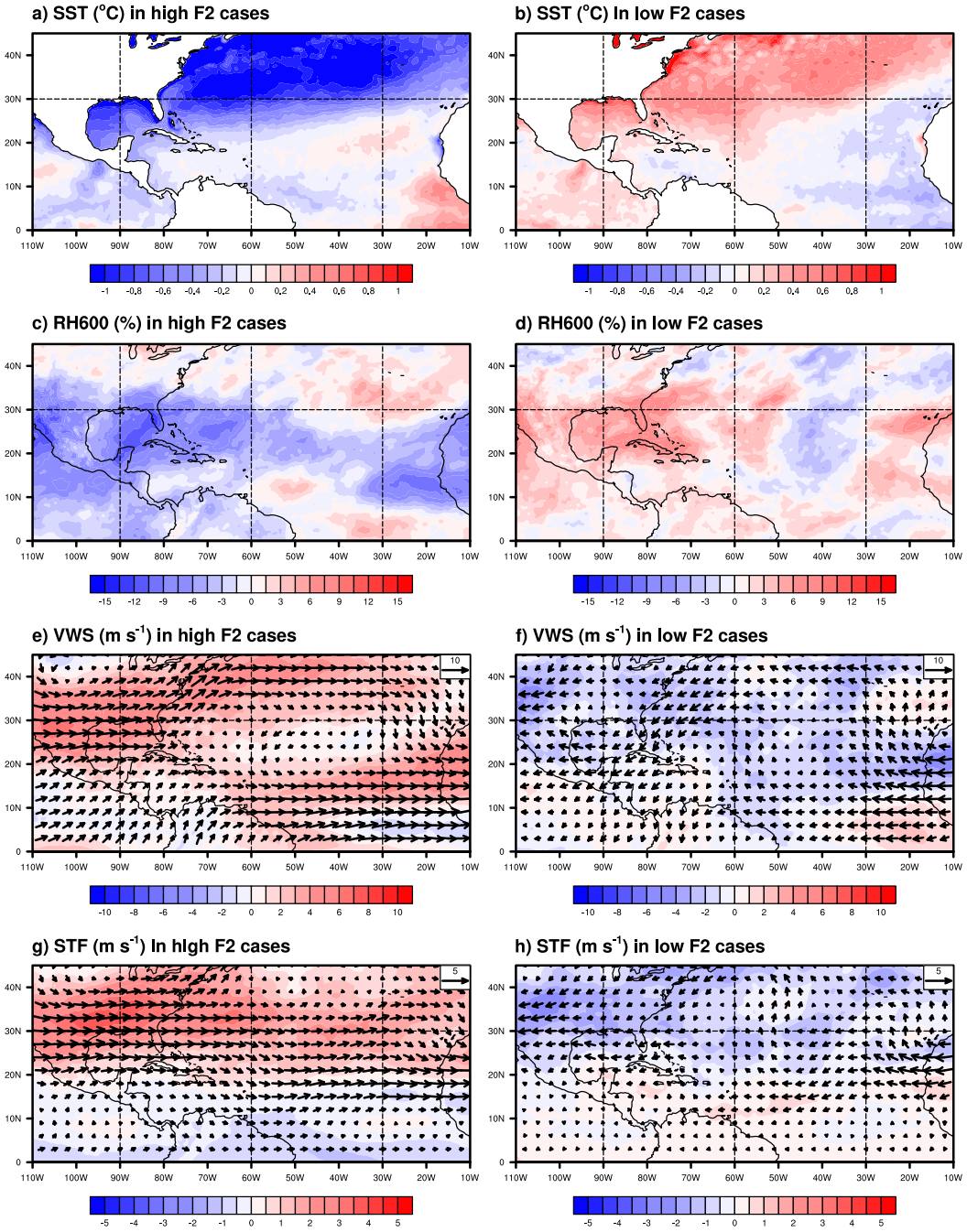

FIG. 7. Climatological anomaly composites of (a),(b) sea surface temperature (SST), (c),(d) RH600, (e),(f) vertical wind shear (VWS), and (g),(h) steering flow (STF) for the (left) high-F2 and (right) low-F2 cases. High-F2 cases are defined as F2 greater than the mean value plus 1 standard deviation of F2. Low-F2 cases are defined as F2 less than the mean value minus 1 standard deviation of F2. Only differences that are significant at the 95% confidence level by Student's *t* test are presented.

mean value minus 1 standard deviation; right column in Fig. 7). Thus, F2 explains variations in environmental flows accompanied with SST and RH600. From our results, F3 (i.e., V_{max}) was observed to be independent of the seven environmental variables (green bars in Fig. 4). In general, V_{max} increased or decreased in developing or decaying stages, respectively, which differs from the variations in environmental conditions. For example, SST is very high in the early stage of TC formation, as TCs are generated over warm tropical oceans. Then, SST gradually decreases as TCs move

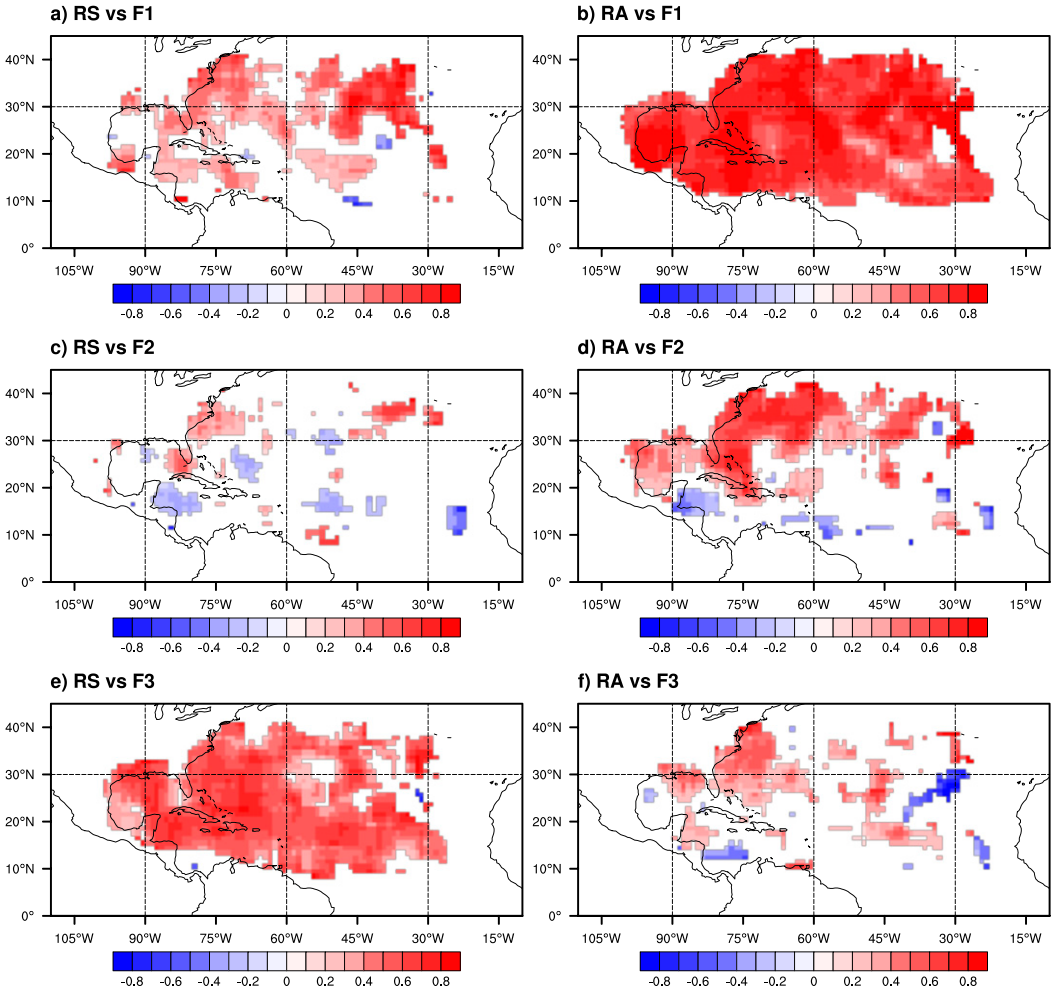

FIG. 8. Correlation coefficients between the three major factors and TC rainfall structure from the TRMM for (left) rainfall strength and (right) rainfall area for the three major factors (a),(b) F1; (c),(d) F2; and (e),(f) F3. Only grid points with correlation coefficients that are significant at the 95% confidence level are shown.

to midlatitudes. Therefore, F3 does not have a strong linear relationship with environmental conditions.

5. Influence of major factors on tropical cyclone rainfall

On the basis of the results from factor analyses, the relationships between TC rainfall (i.e., RS and RA) and the three major factors (F1–F3) were investigated (Figs. 8 and 9). Notably, RS showed a significantly positive relationship with F3 over the entire North Atlantic (Figs. 8e and 9e). On the other hand, relatively weak relationships between RS and F1 appeared over the basin (Figs. 8a and 9a). The relationship between RS and F2 was insignificant for most of the basin (Figs. 8c and 9c). This result confirms that RS is mainly determined by V_{max}, an inherent characteristic of TCs, rather than by large-scale environmental conditions. In contrast, RA showed a significantly positive relationship with F1 over the entire basin (Figs. 8b and 9b). A large F1 value indicates large-scale low pressure systems with high humidity, positive vorticity, convergence in the lower troposphere, and divergence in the upper troposphere, which are favorable conditions for large RAs (Fig. 4). In addition, a positive relationship between RA and F2 was observed in the northwestern section of the North Atlantic (Figs. 8d and 9d) where SST, RH600, and environmental flows varied significantly (Fig. 7). Environmental flows influence RA variation by inducing asymmetric rainfall structure (Kim et al. 2018, 2019), and the dynamic structure of TCs (e.g., intensity and asymmetric convections) can be more sensitive to environmental flows when the TC is weaker (Jones 1995; Wong and Chan 2004). According to F2, SST and RH600 are inversely proportional to environmental flows above 20°N (Fig. 7), meaning that TCs are generally exposed to cooler SSTs and dry condition when environmental flows are stronger. Under these conditions, environmental flows have a strong influence on RA as cooler SSTs and dry condition can weaken TC intensity. A positive relationship between RA and F3 mainly appeared near the eastern part of the United States (Figs. 8f and 9f). Therefore,

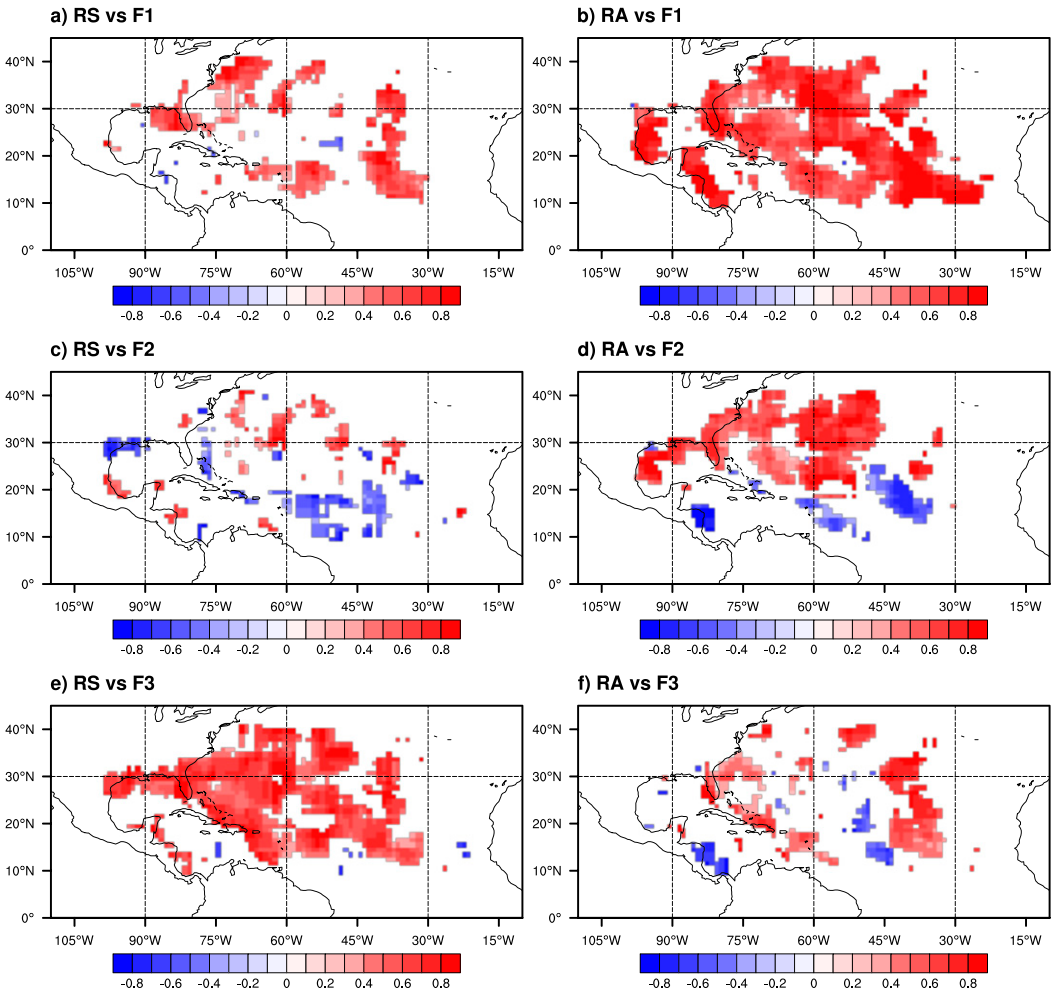

FIG. 9. As in Fig. 8, but for the IMERG.

large-scale low and high pressure systems (i.e., F1) primarily affect RA over the North Atlantic, whereas environmental flows, SST, and RH600 (i.e., F2), as well as V_{max} (i.e., F3), partially contribute to changes in RA in the midlatitudes.

Contributions of the three major factors to the changes in TC rainfall structure were further investigated using multivariable linear regression models for the RS and RA. Because of the difference in precipitation data between the two analysis periods, regression models were constructed for each period. The regression model based on the three major factors accounted for 34.7% and 53.5% of the total variability of RS and RA from the TRMM, respectively, and for 35.7% and 44.2% of the total variability of RS and RA from the IMERG, respectively (Table 3). The largest regression coefficient β was related to F3 (β = 1.04 and 1.43 for the TRMM and IMERG, respectively) in the RS model and F1 (β = 1.62 and 1.23 for the TRMM and IMERG, respectively) in the RA model. This result confirms that the primary factors affecting RS and RA are V_{max} and large-scale low/high pressure systems, respectively. Moreover, the spatial distributions of the mean RS and RA values estimated from the model were similar to those obtained from observations (Fig. 2 vs Figs. 10a,b and 11a,b). The pattern correlation between observation and estimation of mean RS is 0.72 for the TRMM and 0.80 for the IMERG. The pattern correlation between observation and estimation of mean RA is 0.87 for the TRMM and 0.79 for the IMERG. In addition, the correlation coefficients between the observed and estimated RS in each grid box were in the range of 0.23–0.92 for

TABLE 3. Results from multivariable linear regression models with regard to rainfall strength (RS) and rainfall area (RA). The r value represents correlation coefficients between the model and observed data for both RS and RA.

			Regression coef β			
		r^2	F1	F2	F3	Intercept
TRMM	RS model	0.347	0.48	−0.15	1.04	2.88
	RA model	0.535	1.62	0.10	0.27	3.65
IMERG	RS model	0.357	0.81	0.06	1.43	3.45
	RA model	0.442	1.23	0.11	0.27	2.98

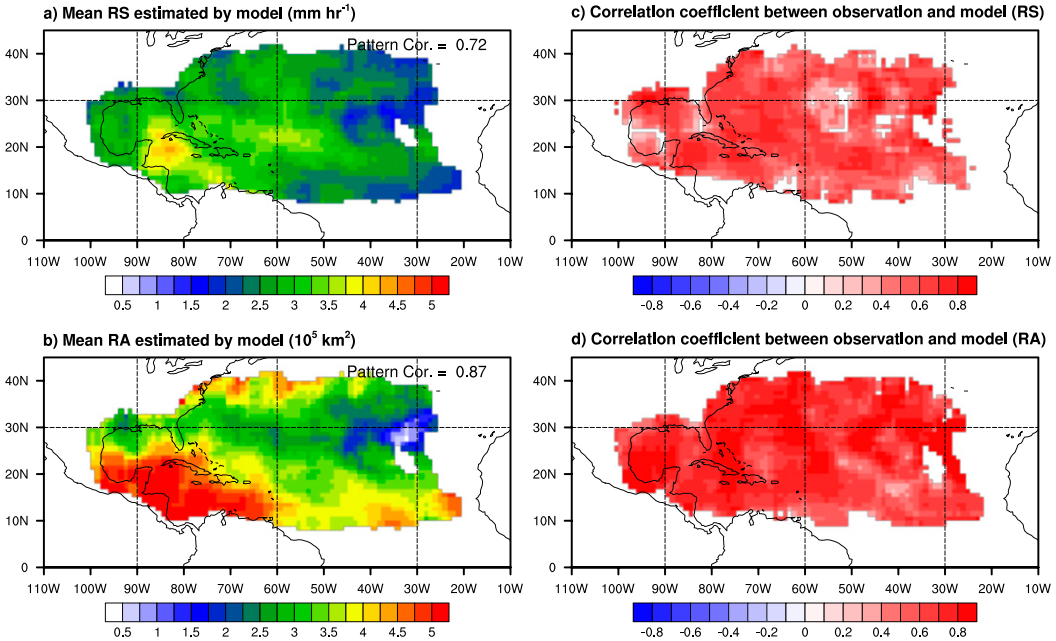

FIG. 10. Mean distributions of (a) rainfall strength and (b) rainfall area estimated using a regression model for the TRMM. Also shown are correlation coefficients between observed and estimated (c) RS and (d) RA in each grid point. Only grid points with correlation coefficients that are significant at the 95% confidence level are presented.

the TRMM and 0.34–0.97 for the IMERG, and the observed and estimated RA in each grid box were in the range of 0.28–0.96 for the TRMM and 0.32–0.96 for the IMERG, and correlations were significant for most parts of the basin (Figs. 10c,d and 11c,d). Accordingly, the regression models are suitable for the estimation of TC rainfall from the three major factors, regardless of region. Therefore, we suggest that the large variability of RS and RA in space can be attributed to the variations in F1–F3.

6. Summary and discussion

In this study, we investigated the influence of large-scale environmental conditions on inner-core rainfall strength and total rainfall area of Atlantic TCs. Both RS (the mean rainfall rate within a 200-km radius from the TC center) and RA (the total area of TC rain cells within a 500-km radius from the TC center) were calculated from TRMM and IMERG precipitation data for the TC season (from July to November) from 1998 to 2014 and 2014 to 2019, respectively. In our results, RS and RA showed a lognormal distribution of occurrence frequency with mean values of 2.88 mm h^{-1} and 3.66×10^5 km^2 for TRMM and 3.46 mm h^{-1} and 2.94×10^5 km^2 for IMERG, respectively. Both indices varied substantially between regions, with large RS values over the Gulf of Mexico, the Caribbean Sea, and east of the West Indies (15°–25°N and 55°–90°W) and large RA over the tropics west of 60°W and midlatitudes near 60°W.

From our results, variations in RS and RA according to the V_{max} and various environmental conditions indicate that RS is strongly correlated with V_{max}, but weakly correlated with large-scale environmental conditions. In contrast, RA showed a stronger correlation with environmental conditions such as RV850, RH600, DV850, and DV200 than with V_{max}. Factor analysis revealed that the seven selected environmental conditions and V_{max} could be combined into three major factors with factor 1 related to large-scale low and high pressure systems over the North Atlantic; factor 2 representing variations in environmental flows, SST, and RH600 that are particularly significant above 20°N; and, last, factor 3 associated with V_{max} and independent of the other environmental conditions. This result indicates that TCs are affected by covarying multiple environmental conditions rather than by single environmental conditions.

In addition, our results showed RS to have a significant positive relationship with F3 over the entire North Atlantic region, whereas the variation of RA was closely related to F1, regardless of region. Furthermore, both F2 and F3 contributed to the changes in RA, particularly over the northwestern part of the North Atlantic. Therefore, we suggest that the primary factor controlling RS is the inherent primary circulation of the TC (i.e., V_{max}; F3), whereas RA is significantly influenced by environmental conditions surrounding TCs, namely large-scale low/high pressure systems (F1) and environmental flows with SST, and RH600 (F2). A multivariable regression model using the three factors explained the variability of the RS and RA by more than 34.7% and 44.2% respectively. Moreover, the model also successfully estimated the spatial distributions of RS and RA in terms of mean values and variations over the entire North Atlantic.

Our results suggest that RS and RA have different characteristics in terms of controlling factors. In other words, the mechanisms controlling TC rainfall in the inner core (RS) and the outer region (RA) may differ and should be investigated in further

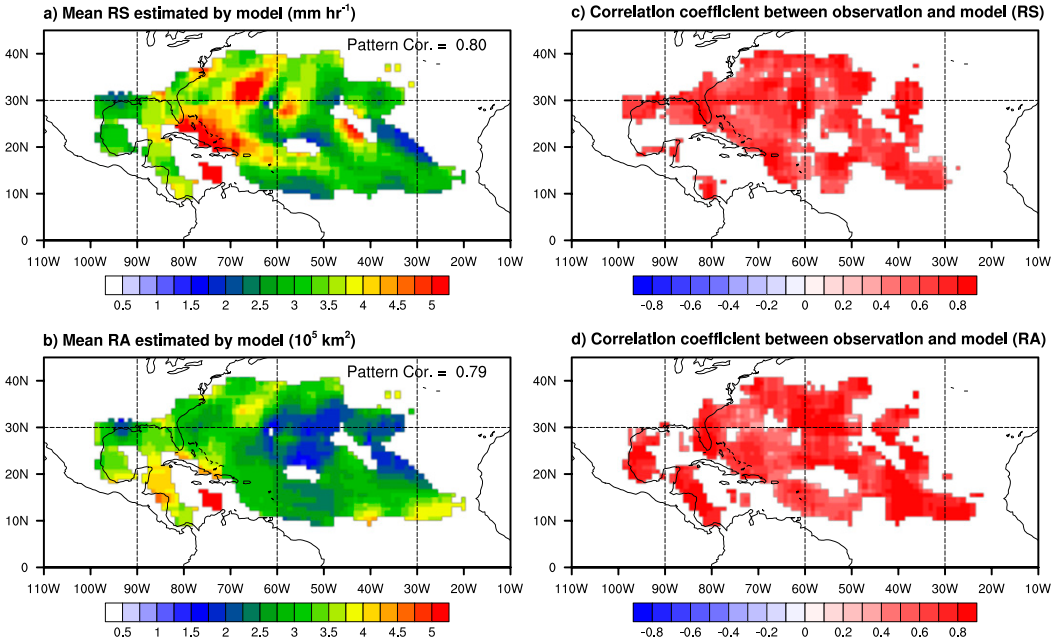

FIG. 11. As in Fig. 10, but for the IMERG.

studies. By quantifying the influence of environmental conditions on TC rainfall, this study may help to improve current forecasting systems for TC rainfall. For example, the predictability of TC rainfall in outer regions could be improved by the inclusion of F1 and F2 in statistical models. Within this context, the dominant time scale for variations in F1 and F2 is also important. Previous studies refer to the influence of the Madden–Julian oscillation (MJO) on TC genesis frequency in the North Atlantic by modulating cyclonic circulation in the Gulf of Mexico (Maloney and Hartmann 2000). Certainly, F1 and related large-scale cyclonic circulations vary significantly according to MJO indices from the Climate Prediction Center of the National Oceanic and Atmospheric Administration, indicating that the MJO is one of the possible factors controlling large-scale environmental conditions that affect TC rainfall (figure not shown). In addition, variations in F2 may be associated with seasonal cycle. The increase in environmental flows accompanied with decrease in sea surface temperature and humidity occurs as a transition from warm to cold season. The mean occurrence date of high-F2 events (26 September) is later than that of low-F2 events (10 September), which is a significant difference at a 95% confidence level. Thus, F2 is likely to be higher in the autumn and lower in the early summer. The relationships between environmental conditions and TC rainfall simulated by numerical models can also be evaluated using our results, which suggests the need to improve the limitations of numerical models.

Acknowledgments. We appreciate two anonymous reviewers whose comments helped to improve and clarify this paper. This work was funded by the Korea Meteorological Administration Research and Development Program under Grant KMI2020-00610 and by the National Research Foundation of the South Korean government (2020R1A4A3079510 and 2020R1C1C1014321).

Data availability statement. All best-track, sea surface temperature, precipitation, and reanalysis data used in this study are openly available from the NOAA National Centers for Environmental Information (https://www.ncdc.noaa.gov/ibtracs/index.php and https://www.ncdc.noaa.gov/oisst), NASA Goddard Earth Sciences Data and Information Services Center (https://disc.gsfc.nasa.gov), and ECMWF (https://cds.climate.copernicus.eu/#!/search?text=ERA5&type=dataset).

REFERENCES

Bakkensen, L. A., D.-S. R. Park, and R. S. R. Sarkar, 2018: Climate costs of tropical cyclone losses also depend on rain. *Environ. Res. Lett.*, **13**, 074034, https://doi.org/10.1088/1748-9326/aad056.

Cerveny, R. S., and L. E. Newman, 2000: Climatological relationships between tropical cyclones and rainfall. *Mon. Wea. Rev.*, **128**, 3329–3336, https://doi.org/10.1175/1520-0493(2000)128<3329:CRBTCA>2.0.CO;2.

Chan, K. T. F., and J. C. L. Chan, 2015: Global climatology of tropical cyclone size as inferred from QuikSCAT data. *Int. J. Climatol.*, **35**, 4843–4848, https://doi.org/10.1002/joc.4307.

Chavas, D. R., and K. A. Emanuel, 2010: A QuikSCAT climatology of tropical cyclone size. *Geophys. Res. Lett.*, **37**, L18816, https://doi.org/10.1029/2010GL044558.

——, N. Lin, and K. Emanuel, 2015: A model for the complete radial structure of the tropical cyclone wind field. Part I: Comparison with observed structure. *J. Atmos. Sci.*, **72**, 3647–3662, https://doi.org/10.1175/JAS-D-15-0014.1.

——, ——, W. Dong, and Y. Lin, 2016: Observed tropical cyclone size revisited. *J. Climate*, **29**, 2923–2939, https://doi.org/10.1175/JCLI-D-15-0731.1.

Chen, S. Y. S., J. A. Knaff, and F. D. Marks, 2006: Effects of vertical wind shear and storm motion on tropical cyclone rainfall asymmetries deduced from TRMM. *Mon. Wea. Rev.*, **134**, 3190–3208, https://doi.org/10.1175/MWR3245.1.

Chen, Y., and M. K. Yau, 2003: Asymmetric structures in a simulated landfalling hurricane. *J. Atmos. Sci.*, **60**, 2294–2312, https://doi.org/10.1175/1520-0469(2003)060<2294:ASIASL>2.0.CO;2.

Corbosiero, K. L., and J. Molinari, 2002: The effects of vertical wind shear on the distribution of convection in tropical cyclones. *Mon. Wea. Rev.*, **130**, 2110–2123, https://doi.org/10.1175/1520-0493(2002)130<2110:TEOVWS>2.0.CO;2.

——, and ——, 2003: The relationship between storm motion, vertical wind shear, and convective asymmetries in tropical cyclones. *J. Atmos. Sci.*, **60**, 366–376, https://doi.org/10.1175/1520-0469(2003)060<0366:TRBSMV>2.0.CO;2.

Czajkowski, J., K. Simmons, and D. Sutter, 2011: An analysis of coastal and inland fatalities in landfalling US hurricanes. *Nat. Hazards*, **59**, 1513–1531, https://doi.org/10.1007/s11069-011-9849-x.

——, G. Villarini, M. Montgomery, E. Michel-Kerjan, and R. Goska, 2017: Assessing current and future freshwater flood risk from North Atlantic tropical cyclones via insurance claims. *Sci. Rep.*, **7**, 41609, https://doi.org/10.1038/srep41609.

DeMaria, M., J.-J. Baik, and J. Kaplan, 1993: Upper-level eddy angular-momentum fluxes and tropical cyclone intensity change. *J. Atmos. Sci.*, **50**, 1133–1147, https://doi.org/10.1175/1520-0469(1993)050<1133:ULEAMF>2.0.CO;2.

Frank, W. M., and E. A. Ritchie, 1999: Effects of environmental flow upon tropical cyclone structure. *Mon. Wea. Rev.*, **127**, 2044–2061, https://doi.org/10.1175/1520-0493(1999)127<2044:EOEFUT>2.0.CO;2.

——, and ——, 2001: Effects of vertical wind shear on the intensity and structure of numerically simulated hurricanes. *Mon. Wea. Rev.*, **129**, 2249–2269, https://doi.org/10.1175/1520-0493(2001)129<2249:EOVWSO>2.0.CO;2.

Fu, B., M. S. Peng, T. Li, and D. E. Stevens, 2012: Developing versus nondeveloping disturbances for tropical cyclone formation. Part II: Western North Pacific. *Mon. Wea. Rev.*, **140**, 1067–1080, https://doi.org/10.1175/2011MWR3618.1.

Hanley, D., J. Molinari, and D. Keyser, 2001: A composite study of the interactions between tropical cyclones and upper-tropospheric troughs. *Mon. Wea. Rev.*, **129**, 2570–2584, https://doi.org/10.1175/1520-0493(2001)129<2570:ACSOTI>2.0.CO;2.

Hersbach, H., and Coauthors, 2020: The ERA5 global reanalysis. *Quart. J. Roy. Meteor. Soc.*, **146**, 1999–2049, https://doi.org/10.1002/qj.3803.

Hill, K. A., and G. M. Lackmann, 2009: Influence of environmental humidity on tropical cyclone size. *Mon. Wea. Rev.*, **137**, 3294–3315, https://doi.org/10.1175/2009MWR2679.1.

Houze, R. A., 2010: Clouds in tropical cyclones. *Mon. Wea. Rev.*, **138**, 293–344, https://doi.org/10.1175/2009MWR2989.1.

Huffman, G. J., and Coauthors, 2007: The TRMM Multisatellite Precipitation Analysis (TMPA): Quasi-global, multiyear, combined-sensor precipitation estimates at fine scales. *J. Hydrometeor.*, **8**, 38–55, https://doi.org/10.1175/JHM560.1.

——, and Coauthors, 2019: GPM IMERG final precipitation L3 half hourly 0.1 degree × 0.1 degree V06. Goddard Earth Sciences Data and Information Services Center (GES DISC), accessed 5 October, https://doi.org/10.5067/GPM/IMERG/3B-HH/06.

Jiang, H., J. B. Halverson, J. Simpson, and E. J. Zipser, 2008a: Hurricane "rainfall potential" derived from satellite observations aids overland rainfall prediction. *J. Appl. Meteor. Climatol.*, **47**, 944–959, https://doi.org/10.1175/2007JAMC1619.1.

——, ——, and E. J. Zipser, 2008b: Influence of environmental moisture on TRMM-derived tropical cyclone precipitation over land and ocean. *Geophys. Res. Lett.*, **35**, L17806, https://doi.org/10.1029/2008GL034658.

Jones, S. C., 1995: The evolution of vortices in vertical shear. I: Initially barotropic vortices. *Quart. J. Roy. Meteor. Soc.*, **121**, 821–851, https://doi.org/10.1002/qj.49712152406.

Kim, D., C.-H. Ho, D.-S. R. Park, J. C. L. Chan, and Y. Jung, 2018: The relationship between tropical cyclone rainfall area and environmental conditions over the subtropical oceans. *J. Climate*, **31**, 4605–4616, https://doi.org/10.1175/JCLI-D-17-0712.1.

——, ——, ——, and J. Kim, 2019: Influence of vertical wind shear on wind- and rainfall areas of tropical cyclones making landfall over South Korea. *PLOS ONE*, **14**, e0209885, https://doi.org/10.1371/journal.pone.0209885.

Kim, J.-H., C.-H. Ho, M.-H. Lee, J.-H. Jeong, and D. Chen, 2006: Large increase in heavy rainfall associated with tropical cyclone landfalls in Korea after the late 1970s. *Geophys. Res. Lett.*, **33**, L18706, https://doi.org/10.1029/2006GL027430.

Kimball, S. K., 2008: Structure and evolution of rainfall in numerically simulated landfalling hurricanes. *Mon. Wea. Rev.*, **136**, 3822–3847, https://doi.org/10.1175/2008MWR2304.1.

——, and M. S. Mulekar, 2004: A 15-year climatology of North Atlantic tropical cyclones. Part I: Size parameters. *J. Climate*, **17**, 3555–3575, https://doi.org/10.1175/1520-0442(2004)017<3555:AYCONA>2.0.CO;2.

Knapp, K. R., M. C. Kruk, D. H. Levinson, H. J. Diamond, and C. J. Neumann, 2010: The International Best Track Archive for Climate Stewardship (IBTrACS). *Bull. Amer. Meteor. Soc.*, **91**, 363–376, https://doi.org/10.1175/2009BAMS2755.1.

Konrad, C. E., and L. B. Perry, 2010: Relationships between tropical cyclones and heavy rainfall in the Carolina region of the USA. *Int. J. Climatol.*, **30**, 522–534, https://doi.org/10.1002/joc.1894.

Lin, Y., M. Zhao, and M. Zhang, 2015: Tropical cyclone rainfall area controlled by relative sea surface temperature. *Nat. Commun.*, **6**, 6591, https://doi.org/10.1038/ncomms7591.

Liu, K. S., and J. C. L. Chan, 2002: Synoptic flow patterns associated with small and large tropical cyclones over the western North Pacific. *Mon. Wea. Rev.*, **130**, 2134–2142, https://doi.org/10.1175/1520-0493(2002)130<2134:SFPAWS>2.0.CO;2.

Lonfat, M., F. D. J. Marks, and S. S. Chen, 2004: Precipitation distribution in tropical cyclones using the Tropical Rainfall Measuring Mission (TRMM) Microwave Imager: A global perspective. *Mon. Wea. Rev.*, **132**, 1645–1660, https://doi.org/10.1175/1520-0493(2004)132<1645:PDITCU>2.0.CO;2.

Maloney, E. D., and D. L. Hartmann, 2000: Modulation of hurricane activity in the Gulf of Mexico by the Madden–Julian oscillation. *Science*, **287**, 2002–2004, https://doi.org/10.1126/science.287.5460.2002.

Matyas, C. J., 2010: Associations between the size of hurricane rain fields at landfall and their surrounding environments. *Meteor. Atmos. Phys.*, **106**, 135–148, https://doi.org/10.1007/s00703-009-0056-1.

——, 2013: Processes influencing rain-field growth and decay after tropical cyclone landfall in the United States. *J. Appl. Meteor. Climatol.*, **52**, 1085–1096, https://doi.org/10.1175/JAMC-D-12-0153.1.

——, 2014: Conditions associated with large rain-field areas for tropical cyclones landfalling over Florida. *Phys. Geogr.*, **35**, 93–106, https://doi.org/10.1080/02723646.2014.893476.

Merrill, R. T., 1984: A comparison of large and small tropical cyclones. *Mon. Wea. Rev.*, **112**, 1408–1418, https://doi.org/10.1175/1520-0493(1984)112<1408:ACOLAS>2.0.CO;2.

Molinari, J., and D. Vollaro, 1989: External influences on hurricane intensity. Part I: Outflow layer eddy angular-momentum fluxes. *J. Atmos. Sci.*, **46**, 1093–1105, https://doi.org/10.1175/1520-0469(1989)046<1093:EIOHIP>2.0.CO;2.

Montgomery, M. T., and R. K. Smith, 2017: Recent developments in the fluid dynamics of tropical cyclones. *Annu. Rev. Fluid Mech.*, **49**, 541–574, https://doi.org/10.1146/annurev-fluid-010816-060022.

Park, D.-S. R., C.-H. Ho, C. C. Nam, and H.-S. Kim, 2015: Evidence of reduced vulnerability to tropical cyclones in the Republic of Korea. *Environ. Res. Lett.*, **10**, 054003, https://doi.org/10.1088/1748-9326/10/5/054003.

Park, S. K., and E. Lee, 2007: Synoptic features of orographically enhanced heavy rainfall on the east coast of Korea associated with Typhoon Rusa (2002). *Geophys. Res. Lett.*, **34**, L02803, https://doi.org/10.1029/2006GL028592.

Peng, M. S., B. Fu, T. Li, and D. E. Stevens, 2012: Developing versus nondeveloping disturbances for tropical cyclone formation. Part I: North Atlantic. *Mon. Wea. Rev.*, **140**, 1047–1066, https://doi.org/10.1175/2011MWR3617.1.

Pielke, R. A., J. Rubiera, C. W. Landsea, M. L. Fernández, and R. Klein, 2003: Hurricane vulnerability in Latin America and the Caribbean: Normalized damage and loss potentials. *Nat. Hazards Rev.*, **4**, 101–114, https://doi.org/10.1061/(ASCE)1527-6988(2003)4:3(101).

Rappaport, E. N., 2000: Loss of life in the United States associated with recent Atlantic tropical cyclones. *Bull. Amer. Meteor. Soc.*, **81**, 2065–2073, https://doi.org/10.1175/1520-0477(2000)081<2065:LOLITU>2.3.CO;2.

——, 2014: Fatalities in the United States from Atlantic tropical cyclones: New data and interpretation. *Bull. Amer. Meteor. Soc.*, **95**, 341–346, https://doi.org/10.1175/BAMS-D-12-00074.1.

Reynolds, R. W., N. A. Rayner, T. M. Smith, D. C. Stokes, and W. Wang, 2002: An improved in situ and satellite SST analysis for climate. *J. Climate*, **15**, 1609–1625, https://doi.org/10.1175/1520-0442(2002)015<1609:AIISAS>2.0.CO;2.

Rios Gaona, M. F., G. Villarini, W. Zhang, and G. A. Vecchi, 2018: The added value of IMERG in characterizing rainfall in tropical cyclones. *Atmos. Res.*, **209**, 95–102, https://doi.org/10.1016/j.atmosres.2018.03.008.

Ritchie, E. A., and R. L. Elsberry, 2003: Simulations of the extratropical transition of tropical cyclones: Contributions by the midlatitude upper-level trough to reintensification. *Mon. Wea. Rev.*, **131**, 2112–2128, https://doi.org/10.1175/1520-0493(2003)131<2112:SOTETO>2.0.CO;2.

Rodgers, E. B., S. W. Chang, and H. F. Pierce, 1994: A satellite observational and numerical study of precipitation characteristics in western North Atlantic tropical cyclones. *J. Appl. Meteor.*, **33**, 129–139, https://doi.org/10.1175/1520-0450(1994)033<0129:ASOANS>2.0.CO;2.

Scoccimarro, E., S. Gualdi, G. Villarini, G. A. Vecchi, M. Zhao, K. Walsh, and A. Navarra, 2014: Intense precipitation events associated with landfalling tropical cyclones in response to a warmer climate and increased CO_2. *J. Climate*, **27**, 4642–4654, https://doi.org/10.1175/JCLI-D-14-00065.1.

Smith, J. A., and M. Montgomery, 2010: Hurricane boundary-layer theory. *Quart. J. Roy. Meteor. Soc.*, **136**, 1665–1670, https://doi.org/10.1002/qj.679.

Smith, R. K., M. T. Montgomery, and N. Van Sang, 2009: Tropical cyclone spin-up revisited. *Quart. J. Roy. Meteor. Soc.*, **135**, 1321–1335, https://doi.org/10.1002/qj.428.

Villarini, G., D. A. Lavers, E. Scoccimarro, M. Zhao, M. F. Wehner, G. A. Vecchi, T. R. Knutson, and K. A. Reed, 2014: Sensitivity of tropical cyclone rainfall to idealized global-scale forcings. *J. Climate*, **27**, 4622–4641, https://doi.org/10.1175/JCLI-D-13-00780.1.

Weatherford, C. L., and W. M. Gray, 1988: Typhoon structure as revealed by aircraft reconnaissance. Part I: Data-analysis and climatology. *Mon. Wea. Rev.*, **116**, 1032–1043, https://doi.org/10.1175/1520-0493(1988)116<1032:TSARBA>2.0.CO;2.

Wong, M. L. M., and J. C. L. Chan, 2004: Tropical cyclone intensity in vertical wind shear. *J. Atmos. Sci.*, **61**, 1859–1876, https://doi.org/10.1175/1520-0469(2004)061<1859:TCIIVW>2.0.CO;2.

Woods, C. M., and M. C. Edwards, 2008: Factor analysis and related methods. *Epidemiology and Medical Statistics*, C. R. Rao, J. P. Miller, and D. C. Rao, Eds., Handbook of Statistics Series, Vol. 27, Elsevier, 367–394.

Xu, W., H. Jiang, and X. Kang, 2014: Rainfall asymmetries of tropical cyclones prior to, during, and after making landfall in South China and Southeast United States. *Atmos. Res.*, **139**, 18–26, https://doi.org/10.1016/j.atmosres.2013.12.015.

Zhou, Y., and C. J. Matyas, 2018: Spatial characteristics of rain fields associated with tropical cyclones landfalling over the western Gulf of Mexico and Caribbean Sea. *J. Appl. Meteor. Climatol.*, **57**, 1711–1727, https://doi.org/10.1175/JAMC-D-18-0034.1.

——, ——, H. Li, and J. Tang, 2018: Conditions associated with rain field size for tropical cyclones landfalling over the eastern United States. *Atmos. Res.*, **214**, 375–385, https://doi.org/10.1016/j.atmosres.2018.08.019.